



Contents lists available at ScienceDirect

Computers and Electrical Engineering

journal homepage: www.elsevier.com/locate/compeleceng



Robust precise trajectory tracking of hybrid stepper motor using adaptive critic-based neuro-fuzzy controller[☆]

P. Ghanooni^a, A.M. Yazdani^{b,*}, A. Mahmoudi^c, S. MahmoudZadeh^d, M. Ahmadi Movahed^e, M. Fathi^f

^a Department of Electrical Engineering, Islamic Azad University, Mashhad Branch, Mashhad, Iran

^b College of Science, Health, Engineering and Education, Murdoch University, Perth, WA 6150, Australia

^c College of Science and Engineering, Flinders University, Adelaide, SA 5042, Australia

^d School of Information Technology, Deakin University, Geelong, VIC 3220, Australia

^e Department of Electrical Engineering, Islamic Azad University, Science and Research Branch, Tehran, Iran

^f Faculty of Electrical Engineering, Universiti Teknologi Malaysia, Johor Bahru 81310, Malaysia



ARTICLE INFO

Article history:

Received 7 May 2019

Revised 27 November 2019

Accepted 27 November 2019

Available online 13 December 2019

Keywords:

Adaptive critic-based neuro-fuzzy controller (ACNFC)

Model-free controller

Hybrid stepper motor (HSM)

Speed tracking

Uncertainty

ABSTRACT

In this paper, an adaptive critic-based neuro-fuzzy controller (ACNFC) is developed for robust and high-precision speed trajectory tracking of a hybrid stepper motor (HSM). The proposed model-free controller uses the critic-based learning and backpropagation of errors for adaptive tuning of the consequence part of the fuzzy inference rule. This makes the ACNFC reconfigurable and robust in high-precision tracking applications, such as robot-assisted surgery, involving with parametric uncertainties and environmental disturbances. To investigate the performance and robustness of the ACNFC, HSM system is simulated under various conditions in MATLAB/Simulink. These operating conditions consider mechanical parameter variations, load disturbance, noise impact, and sudden fault occurrence. To verify the effectiveness of the proposed controller, test results are compared with the results obtained by optimized-PI and brain emotional learning-based intelligent controllers. Simulation results confirm the effective performance of the ACNFC for adaptive and precise speed response as well as dealing with nonlinearity and uncertainty in realistic applications.

© 2019 Elsevier Ltd. All rights reserved.

1. Introduction

Hybrid stepper motors (HSMs) are increasingly being used in recent cutting-edge technology applications in which high efficiency, durability, and high precision are required. Examples of these realms are high-performance control of antenna in telecommunication domains, high-precision control of a robot-assisted surgery in biomedical application, high-precision control of a tuneable-laser system, and combustion engine control in automotive engineering applications [1,2].

Stepper motors are generally implemented in an open loop configuration in which a rectangular train of pulses manages the operation. In such a configuration, no information of the motor shaft position or speed is provided, and the motor movement is driven by a pulse train with a pre-determined time interval. However, in an open-loop control strategy and

[☆] This paper is for regular issues of CAEE. Reviews processed and recommended for publication to the Editor-in-Chief by Guest Editor Dr. Shuai Liu.

* Corresponding author.

E-mail address: amirmehdi.yazdani@murdoch.edu.au (A.M. Yazdani).

particularly when the HSM is experiencing fast excitation changes, the HSM may lose its steps, synchronization, and stability and the HSM speed response may suffer from oscillation. This open-loop configuration consequently results in a permanent error between the load position/speed and expected value and therefore the rotor is unable to move to the new demanded position/speed [2,3].

Thus, closed-loop configuration is required to obtain the information on losing step or oscillation occurrence for upgrading the accuracy of trajectory tracking control by reducing the sensitivity against unforeseen variations [4]. Various feedback control methods have been developed to improve the performance of stepper motors for effective and precise trajectory tracking, in particular reducing resonances in low speed regions and vibrations in high speed operating areas [5,6]. A basic closed-loop control approach, named feedback linearization, in which the dynamic of stepper motor was linearized around its operating point, was offered [6]. The test results were superior to that of an open-loop control technique. The scheme suffered from the lack of adaptation for different operating points. Self-tuning regulator was developed as an adaptive strategy to cover the insufficiency of the mentioned non-adaptive solution [7]. However, because of a large amount of floating-point computations which results in higher sampling period, this approach was not suitable for practical implementations. To avoid the HSM resonance at low speeds and vibration at high speeds, several closed-loop micro-stepping-based schemes have been developed [8,9]. However, their performances are limited to just one speed region (either low or medium and high speeds) rather than a wide speed range. Nonlinear control approaches such as sliding mode control (SMC) were used to damp out the resonance and vibration of the stepper motor [10]. SMC can guarantee acceptable accuracy and robustness in dealing with HSM uncertainties. Employing an observer for estimating the load torque was used as a common strategy to diminish the load torque impacts. Combination of the SMC and SMC-based observers effectively eliminated the torque ripples caused by the nonlinear characteristics of the stepper motor.

Fuzzy logic, neural network, and biologically inspired learning techniques were used for stepper motors control [11–15] to achieve the ability of uncertainty handling and learning the dynamic behavior of the complex nonlinear systems. These methods improve the stability in transient dynamics and the tracking characteristics during the speed response by reducing torque ripples and disturbances. For example, a model-free controller based on emotional learning algorithm called brain emotional learning-based intelligent controller (BELBIC) was used for high performance speed tracking of the HSM [15]. Results of this study showed the effectiveness and capability of BELBIC for uncertainty handling in the HSM speed tracking. A laboratory fuzzy-logic controller relying on a 16-bit micro controller was developed and the results showed distinct advantages of the method over traditional adaptive control methods [16]. Lack of systematic approach in designing membership functions and arranging the inference rules was the main difficulty. An artificial neural network structure was employed for precise profile tracking in stepper motor [17]. The scheme showed good performance for speed tracking of stepper motor with success in tackling the problem of system's dynamic variations and disturbance rejection. However, the suggested approach required a large amount of computations for training and adaptation.

In this study, an ACNFC is developed to provide high-precision and robust speed trajectory tracking of the HSM. Compared to the conventional neuro-fuzzy controllers, the ACNFC is computationally efficient and structurally flexible. Structure of the critic provides the online tuning of the controller and evaluates the system status by active exploration of the states based on the feedback outputs. It provides rewards and punishments as per the states which system observes. The critic-based learning methods are very flexible, as critics constitute less informative learning source. These approaches, called reinforcement-learning methods, consist of an active exploration of the state and action spaces to find what action to apply in each state [18]. They have been employed and used in different realms of research such as controlling a steam generator water level [19], load-frequency control of interconnected power systems [20], and nuclear reactor power control [21].

The main contribution of this paper is to accommodate the problem of precise and robust speed tracking of the HSM quantified in terms of rise time, settling time, recovery time, steady-state error (SSE), undershoot, and overshoot. The aim is to employ the ACNFC to effectively work over the full speed range with at most $\pm 2.5\%$ tracking error with respect to the set point trajectory under various operating conditions such as sudden load torque and noise impact. To the best of authors' knowledge, the ACNFC has not been used in the literature of the HSM control. The focus is therefore on the design and development of this controller which can improve the transient/steady-state response. Due to the learning ability of the proposed approach, the approach is robust and capable to adapt quickly with varying operating conditions.

The main rational to use the ACNFC is because of following salient properties:

- The ACNFC benefits from both the neural network and fuzzy structures, which can express human experts in the form of linguistic variables. In addition, neuro-fuzzy controllers can generate fuzzy rules which can help us to identify the unknown system;
- The ACNFC benefits from reinforcement learning compared to supervisory learning approaches, to online assess the output value. The critic-based structure can help the controller to address any uncertainty which may exist in the system;
- Due to use of critic structure, computational burden for parameter adaptation compared to the conventional neuro-fuzzy controllers is remarkably reduced making the ACNFC desirable for real-time applications.

The abovementioned properties of the ACNFC helps us to overcome difficulties/gaps which have not been thoroughly addressed in the literature of high-precision HSM speed tracking as listed below:

- In high speed or when a large step increment is applied to the HSM, overshoot, loose of steps and accordingly stability and synchronization might happen;

Table 1
HSM parameters.

Rated voltage (volt)	5	Torque constant	0.153
Phase resistance (ohm)	0.37	Rotor inertia (Kg.m ²)	15.62e-5
Phase inductance (mH)	0.9	Step angle (degree)	1.8
Number of rotor teeth	50	Detent torque (Nm)	0.002
Number of phases	2	Coefficient of viscous friction (Nm.s/rad)	0.0001

- In certain speed rate or under certain load torque conditions, HSM usually experiences resonance and vibration phenomena;
- Due to the non-sinusoidal flux distribution in the air gap, non-uniformity in the generated torque occurs which causes speed oscillations and consequently deteriorates the HSM performance especially at low speed operating regions;
- In high performance HSM applications, the control system should not require either high gains in the inner speed/position control loops or restriction of model uncertainties to be modeled by finite-dimensional linear or non-linear exosystems with known dimension.

To show the effectiveness and robustness of the ACNFC for the HSM speed tracking, extensive simulation tests are performed under ideal and perturbed situations. These operating conditions encapsulate, load disturbance, mechanical parameter variations, sudden motor phase interruption, and noise impact. The HSM dynamic model (including driver module) and ACNFC controller are simulated in MATLAB/ Simulink under abovementioned operating conditions. Two benchmark controllers namely an optimized-PI and BELBIC are also used for the performance comparison as well as the ACNFC transient and steady state responses validation.

The rest of this paper is organized as follows. In Section II, the HSM dynamic model and strategy of the field-oriented control is presented. Section III demonstrates the structure of the ACNFC in details. In section IV, simulation studies of the ACNFC performance under various operating conditions are presented. Finally, Section V, provides the conclusion.

2. HSM model

2.1. Fundamental model

The mathematical presentation of the HSM is based on the nonlinear dynamic of the electrical and mechanical subsystems as follows [22]:

$$\begin{aligned} \frac{di_a}{dt} &= \frac{1}{L}[V_a - Ri_a + K_m\omega \sin(N_{rt}\theta)] \\ \frac{di_b}{dt} &= \frac{1}{L}[V_b - Ri_b + K_m\omega \cos(N_{rt}\theta)] \end{aligned} \quad (1)$$

$$\begin{aligned} \frac{d\omega}{dt} &= \frac{K_m}{J}[-i_a \sin(N_{rt}\theta) + i_b \cos(N_{rt}\theta)] - \frac{F}{J}\omega - \frac{T_L}{J} \\ \frac{d\theta}{dt} &= \omega \end{aligned} \quad (2)$$

where θ represents the angular position of the rotor, ω is angular velocity of the rotor, i_a represents current in winding A, and i_b is current in winding B, V_a and V_b are voltages of phases A and B, J is inertia of the rotor, F is viscous friction coefficient, K_m is motor torque constant, R is resistance of the phase winding, L is inductance of the phase winding, N_{rt} is number of rotor teeth, and finally T_L indicates load torque. Table 1 lists the parameters of the HSM in this study.

2.2. Park transformation

In electrical machines and drive modelling, park transformation is employed to provide a new coordinate system which results in a linear relationship between control variables and torque. It transforms vector (v) and (i) carried in the fixed stator frame (a,b) into vectors carried in a new frame called direct-quadrature (d,q) that rotates along the fictitious excitation vector [22]. The d-q relationships for the phase voltages and currents are:

$$\begin{bmatrix} i_d \\ i_q \end{bmatrix} = \begin{bmatrix} \cos(N_{rt}\theta) & \sin(N_{rt}\theta) \\ -\sin(N_{rt}\theta) & \cos(N_{rt}\theta) \end{bmatrix} \begin{bmatrix} i_a \\ i_b \end{bmatrix} \quad (3)$$

$$\begin{bmatrix} V_d \\ V_q \end{bmatrix} = \begin{bmatrix} \cos(N_{rt}\theta) & \sin(N_{rt}\theta) \\ -\sin(N_{rt}\theta) & \cos(N_{rt}\theta) \end{bmatrix} \begin{bmatrix} V_a \\ V_b \end{bmatrix} \quad (4)$$

A new representation of state-space model of the HSM is provided accordingly:

$$\begin{aligned}\frac{di_d}{dt} &= -\frac{R}{L}i_d + N_{rt}\omega i_q + \frac{V_d}{L} \\ \frac{di_q}{dt} &= -\frac{R}{L}i_q - N_{rt}\omega i_d - \frac{K_m}{L}\omega + \frac{V_q}{L} \\ \frac{d\omega}{dt} &= \frac{K_m}{J}i_q - \frac{F}{J}\omega + \frac{T_L}{J} \\ \frac{d\theta}{dt} &= \omega\end{aligned}\tag{5}$$

2.3. Field oriented control

Field Oriented Control (FOC) is used for independent control of the motor's flux and torque. The d-axis is chosen on the flux axis so that the flux lines are aligned with this axis. The torque is controlled by controlling the current in the q-axis. In the FOC principle, d-axis is set to be zero in order to provide the maximum output torque. Therefore, the direct current i_d is set to zero and the developed torque is a component of quadrature current, as shown in (6). In other words, the output of the controller, produced based on the variations of speed error, is of the torque component (i_q^*). The HSM driver, includes hysteresis current controllers, which are simulated by means of relay blocks in MATLAB/ Simulink, and PWM convertors modelled by MOSFET-Diode H-bridges. Two hysteresis current controllers are responsible for producing the gate pulses of the convertor. The synchronous reference frame currents (i_d^*, i_q^*) are transformed into reference phase currents (i_{aref}, i_{bref}) and the aftereffect of the comparison between the reference and actual currents are directed through the hysteresis controllers. These modifications are performed in accordance with the Clark and Park transformations. In the first place, the synchronous frame (i_d^*, i_q^*) is transformed into the stationary frame (i_d^s, i_q^s) based on the inverse Park formula in (7) and then it is converted into a reference frame (i_{aref}, i_{bref}) based on the Clark inverse formula in (8).

$$T = K_m \cdot i_q^* \tag{6}$$

$$\begin{bmatrix} i_d^s \\ i_q^s \end{bmatrix} = \begin{bmatrix} \cos(N_{rt}\theta) & -\sin(N_{rt}\theta) \\ \sin(N_{rt}\theta) & \cos(N_{rt}\theta) \end{bmatrix} \begin{bmatrix} i_d^* \\ i_q^* \end{bmatrix} \tag{7}$$

$$\begin{bmatrix} i_{aref} \\ i_{bref} \end{bmatrix} = \begin{bmatrix} 1 & 0 \\ -1/2 & \sqrt{3}/2 \end{bmatrix} \begin{bmatrix} i_d^s \\ i_q^s \end{bmatrix} \tag{8}$$

Fig. 1 shows the two H-Bridge converters employed to drive the HSM. Each converter comprises of two arms constructed with MOSFET and diode. The required pulses, N_a and N_b , for the gates excitation are generated based on the current error in hysteresis loops. The phase voltages V_a and V_b , consequently, are constructed with respect to the (9) and (10), in which V_{dc} is the DC-link voltage. **Fig. 2** illustrates the block diagram of the HSM drive as per the FOC principle.

$$v_a = \frac{V_{dc}}{2}[2N_a - 1] \tag{9}$$

$$v_b = \frac{V_{dc}}{2}[2N_b - 1] \tag{10}$$

3. Adaptive critic-based neuro-fuzzy controller

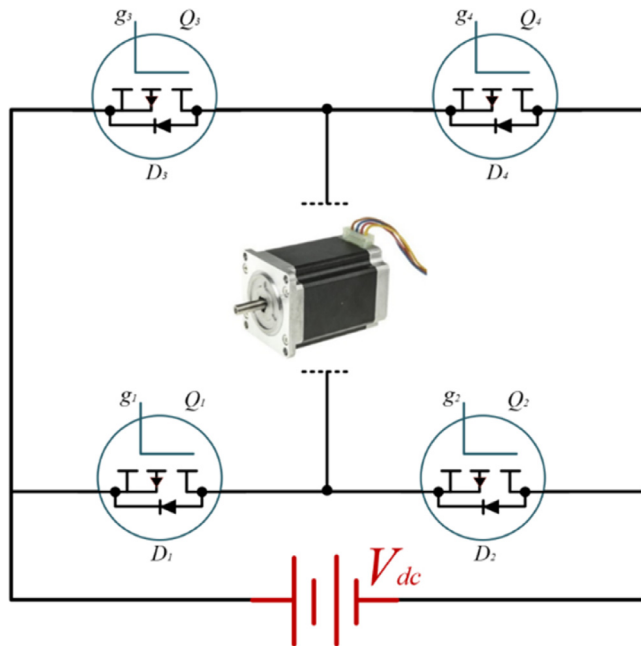
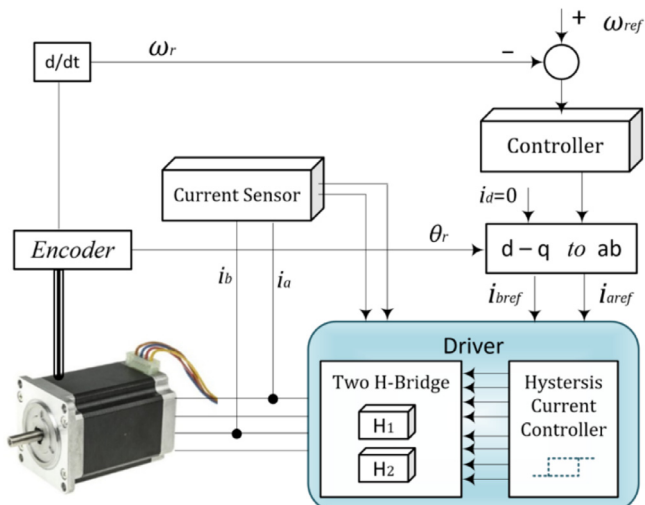
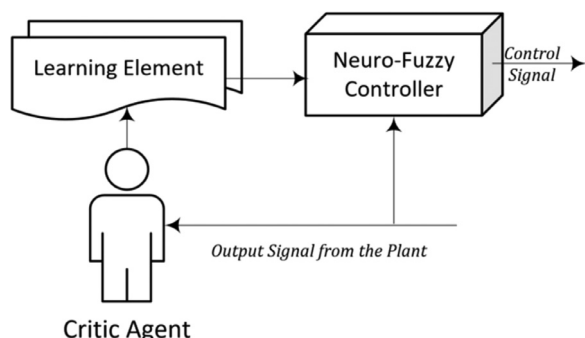
In this section, principle of the ACNFC is described in detail. The ACNFC contains two main blocks namely neuro-fuzzy and critic (called critic agent). **Fig. 3** shows the architecture of the ACNFC. In this particular controller, reinforcement-learning concept is employed to design an adaptive critic. The critic signal is used for continuously updating the parameters of neuro-fuzzy architecture. In the subsequent sub-sections, details of the neuro-fuzzy system and critic structure are explained.

3.1. Neuro-fuzzy system

The terminology of neuro-fuzzy in the literature is usually interpreted as an architecture incorporating fuzzy system concept into an adaptive neural network concept [19]. Fuzzy systems, in principle, are real nonlinear mapping systems from the input vector $X = [x_1, x_2, \dots, x_n]^T \in \mathbb{R}^n$ to an output vector $\tilde{y} = \tilde{f}(X) \in \mathbb{R}^m$, where n and m denote the input and output vector dimensions, respectively. Two types of fuzzy systems called Takagi-Sugeno-Kang (TSK) and Mamdani are more common in the literature. The neuro-fuzzy system in this study is established upon the TSK type.

Let us consider a multiple-input, single-output (MISO) fuzzy system consisting of N rules as follows:

$$R_j : \text{if } (x_1 \text{ is } F_{j1}) \text{ and } (x_2 \text{ is } F_{j2}) \text{ and } \dots \text{ and } (x_n \text{ is } F_{jn}) \text{ then } c_j = g_j(X)$$

**Fig. 1.** MOSFET-diode H-bridge convertor.**Fig. 2.** Block diagram of HSM drive with respect to the FOC principle.**Fig. 3.** Architecture of the ACNFC.

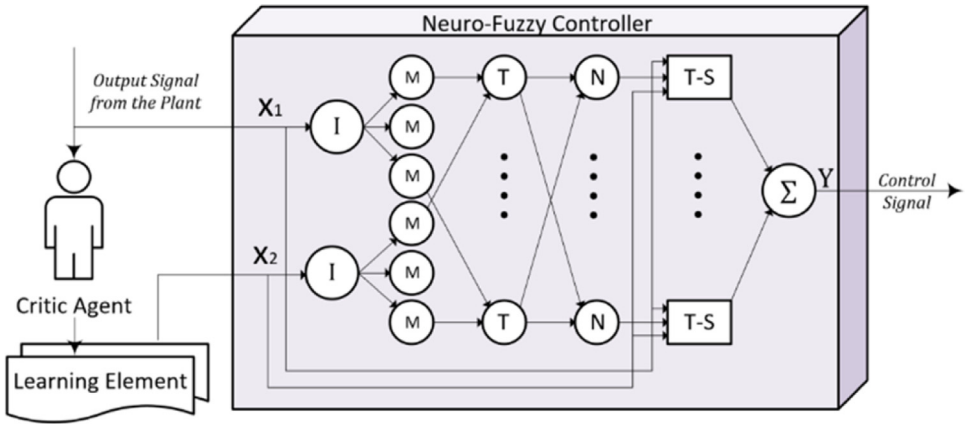


Fig. 4. Architecture of the neuro-fuzzy system based on the TSK inference system.

where $j = 1, 2, \dots, N$ and R_j is representation of j^{th} rule in the fuzzy inference engine; x_i ($i = 1, 2, \dots, n$) are the input variables of the fuzzy system, F_{ji} is a fuzzy set defined by a membership function of $\mu_{F_{ji}}(x_i)$, c_j is the consequence of the j^{th} rule and $c_j: \Re^n \rightarrow \Re^m$ is a linear or nonlinear function. The antecedent fuzzy set of each rule, that is fuzzy Cartesian product $F_{j1} \times F_{j2} \times \dots \times F_{jn}$, is quantified by the t-norm of min or product as defined in (11) and the defuzzification process is performed by (12).

$$\mu_{F_{j1}, \dots, F_{jn}}(x_1, \dots, x_n) = \begin{cases} \min [\mu_{F_{j1}}(x_1), \dots, \mu_{F_{jn}}(x_n)] \\ \text{or} \\ \mu_{F_{j1}}(x_1) \times \dots \times \mu_{F_{jn}}(x_n) \end{cases} \quad (11)$$

$$\tilde{u} = \tilde{f}(X) = \frac{\sum_{j=1}^N c_j \mu_j}{\sum_{j=1}^N \mu_j}, \quad X = [x_1, \dots, x_n]^T \in \Re^n \quad (12)$$

In (12), μ_j represents the firing strength of the antecedent part of the j^{th} rule that is defined by (13).

$$\mu_j = \mu_{F_{j1} \times \dots \times F_{jn}}(x_1, \dots, x_n) \quad (13)$$

In the proposed TSK fuzzy system, the consequent part of rules is obtained by (14):

$$c_j = a_{0j} + \sum_{i=1}^n a_{ij} x_i \quad (14)$$

where a_{0j} and a_{ij} coefficients are design parameters normally tuned during the learning phase.

A six-layer neuro-fuzzy network is developed by implementation of a fuzzy inference system in the framework of an adaptive neural network. The neuro-fuzzy system has two-input and one-output TSK fuzzy inference system with three linguistic variables for each input and consequently nine rules for inferencing process. It is noted that each layer of the neuro-fuzzy network is served as one part of the equivalent fuzzy system. Fig. 4 illustrates the architecture of the proposed neuro-fuzzy system.

In Fig. 4, in the first layer, each node denoted by I is a scaling factor to normalize each input into the range of $[-1, 1]$. In the second layer, nodes labeled by M, specify the degree of membership functions to transform real input variable into linguistic variables. In the third layer, nodes denoted by T, provide the antecedent part of fuzzy rules, $(\mu_{F_{j1}}(x_1) \times \dots \times \mu_{F_{jn}}(x_n))$, by multiplying the incoming variables from layer two. In the fourth layer, nodes labeled by N, are responsible for calculating the ratio of firing strength in the j^{th} node to sum of all rules firing strengths, i.e., $\mu_j / \sum_{j=1}^N \mu_j$. In the fifth layer, the blocks denoted by T-S, are representatives of TSK rules and the consequent part of these rules is calculated based on a linear combination of the inputs and adding a constant value as defined in (14). Note that the coefficients of the linear combinations and the constant value are updated during the learning stage. Finally, in the sixth layer, the defuzzification operator is applied to calculate the output of the network, as indicated in (12).

3.2. Controller structure

The ACNFC performance is controlled by a critic agent unit based on assessment of the output feedback of an underlying system and generating an appropriate reinforcement signal, $r \in [-1, 1]$ (see Fig. 4). The reinforcement signal contributes effectively by updating parameters of the neuro-fuzzy network. The control objective is to minimize the reinforcement signal to achieve zero value (terminating the learning process). This is provided by the learning element employed to adapt tunable parameters of the controller.

Let us define the cost function using (15). The main objective of the learning procedure is to minimize the cost function in (15), by updating the neuro-fuzzy controller parameters in the opposite direction of the gradient of the cost function, formulated in (16):

$$E = \frac{1}{2} r^2 \quad (15)$$

$$\Delta w = -\eta \cdot \frac{\partial E}{\partial w} \quad (16)$$

where η and w are the learning rate and tunable parameter of the neuro-fuzzy controller, respectively. Then, the chain rule is applied to obtain partial derivative of (16):

$$\frac{\partial E}{\partial w} = \frac{\partial E}{\partial w} \cdot \frac{\partial r}{\partial u} \cdot \frac{\partial u}{\partial w} \quad (17)$$

where u represents the control signal.

Let us define the reinforcement signal as (18):

$$r = k_1 \cdot e + k_2 \cdot \dot{e} \quad (18)$$

where k_1 , and k_2 are positive weighting coefficients highlighting the importance of each terms in (18) and the error signal (e) is defined by $e = y_{ref} - y$ where y is the actual output of the system and y_{ref} is the reference signal.

Now, by substituting (15) in (17), we have:

$$\frac{\partial E}{\partial w} = r \cdot \frac{\partial r}{\partial y} \cdot \frac{\partial y}{\partial u} \cdot \frac{\partial u}{\partial w} \quad (19)$$

where

$$\frac{\partial r}{\partial y} = \frac{\partial r}{\partial e} \cdot \frac{\partial e}{\partial y} = -k_1 \quad (20)$$

and by using (20), Eq. (19) is rearranged as (21):

$$\frac{\partial E}{\partial w} = r \cdot (-k_1) \cdot \frac{\partial y}{\partial u} \cdot \frac{\partial u}{\partial w} \quad (21)$$

In (21), the term $\partial y / \partial u$ represents steady-state variations of the system output to the control signal. The system is designed such that the sign of this variation should be positive that is sufficient for the adaptation rule. The adaptation rule of the tunable parameter is then calculated as (22).

$$\Delta w = \eta \cdot r \cdot k_1 \cdot \frac{\partial u}{\partial w} \quad (22)$$

By using (12) and (14), the control signal for the neuro-fuzzy controller introduced in the previous sub-section is obtained as (23):

$$u = \frac{\sum_{j=1}^N (a_{0j} + \sum_{j=1}^N a_{ij}x_i) \mu_i}{\sum_{j=1}^N \mu_j} \quad (23)$$

Accordingly, the update rules for the parameters of the neuro-fuzzy controller are provided by (24) and (25).

$$\Delta a_{0j} = \eta \cdot r \cdot \frac{\partial u}{\partial a_{0j}} = \eta \cdot r \cdot \frac{\mu_j}{\sum_{j=1}^N \mu_j} \quad (24)$$

$$\Delta a_{1j} = \eta \cdot r \cdot \frac{\partial u}{\partial a_{1j}} = \eta \cdot r \cdot x_i \cdot \frac{\mu_j}{\sum_{j=1}^N \mu_j} \quad (25)$$

3.3. ACNFC for the HSM trajectory tracking

The ACNFC developed for the HSM trajectory tracking, uses HSM speed error and its derivative as inputs and assigns three membership functions of negative (NE), zero (ZE), and positive (PO) for each input (as shown in Fig. 5). It uses nine rules in the fuzzy rule base accordingly. The Sigmoid functions are used for linguistic variables of NE and PO and the Gaussian function is employed for the variable Z, as defined in (26) and (27):

$$\mu(x) = \frac{1}{1 + e^{-a(x-b)}} \quad (26)$$

$$\mu(x) = e^{-(x-c)/\sigma^2} \quad (27)$$

where a , b , c , and σ are curve inflection parameters.

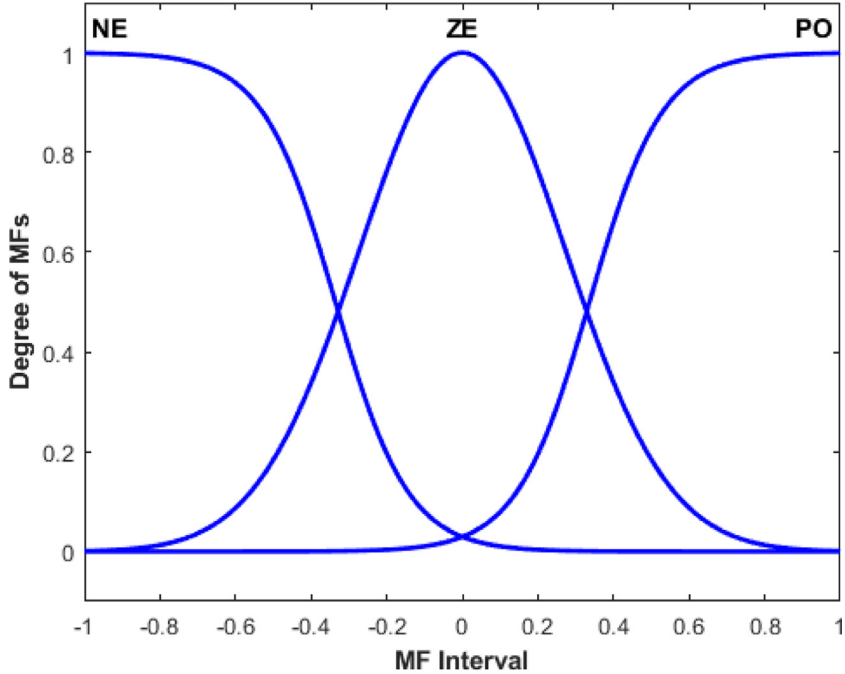


Fig. 5. Membership functions of ACNFC inputs.

In the proposed ACNFC, the critic plays a substantial role. It is, principally, responsible for evaluation of situations, not necessarily too accurate. The critics contributes to tuning the neuro-fuzzy controller parameters so that a desired performance is achievable. In this study, a linear combination of HSM speed error and its derivative is selected as a candidate function for the critic signal, as indicated in Eq. (18). The critic's evaluation of states is performed in such a manner that, for example, if the speed error and its derivative are PO, the critic should evaluate this as an unsatisfactory system performance. Conversely, if the speed error is PO and its derivative is NE, the critic considers this situation as an acceptable performance and expects better performance in the future. These linguistic explanations demonstrate the fuzzy nature of the critic itself.

The proposed neuro-fuzzy controller has two inputs and employs nine rules in the fuzzy rule base whose consequent part are adaptive. The parameters of the neuro-fuzzy controller in this study are updated by (28), (29), and (30).

$$\Delta a_{0j} = \eta \cdot r \cdot \frac{\mu_j}{\sum_{j=1}^9 \mu_j} \quad (28)$$

$$\Delta a_{1j} = \eta \cdot r \cdot e \cdot \frac{\mu_j}{\sum_{j=1}^9 \mu_j} \quad (29)$$

$$\Delta a_{2j} = \eta \cdot r \cdot \dot{e} \cdot \frac{\mu_j}{\sum_{j=1}^9 \mu_j} \quad (30)$$

4. Simulation results

To evaluate the performance of the ACNFC, extensive simulation tests were executed in MATLAB/Simulink under various operating conditions. These simulations examine the ACNFC performance under the startup operation, load-torque disturbance, model parameter variations, noise and offset signal on the HSM drive, and sudden phase interruption. Simulation results are compared to those of optimized-PI controller and BELBIC as benchmark controllers for verification of ACNFC competency. The details of the optimized-PI controller based on the imperialist competitive algorithm (with the gains of $K_p = 2$ and $K_i = 0.343$) and BELBIC controller are found in [15,23,24]. Discussion of simulation results and scenarios are as follow.

4.1. Scenario I: startup

Startup scenario demonstrates the response of the ACNFC to the speed reference signal of 50 rad/s under no-load condition. Fig. 6 demonstrates the significant performance of the ACNFC during startup in terms of control performance indices such as rise time (fast speed response), no overshoot, and no SSE. The speed response generated by the ACNFC can meet

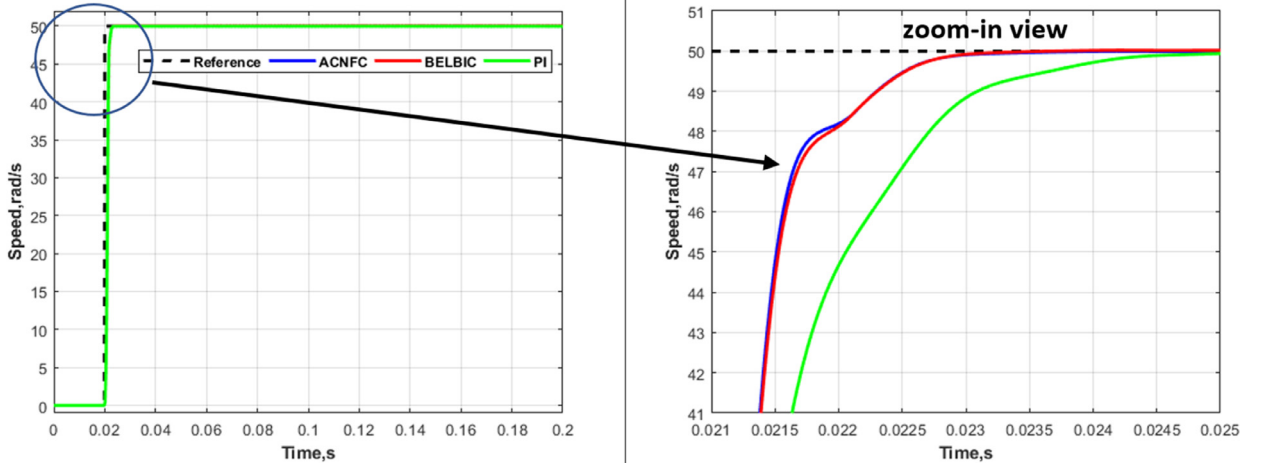


Fig. 6. Startup response of the ACNFC, BELBIC and optimized-PI controllers under no-load condition.

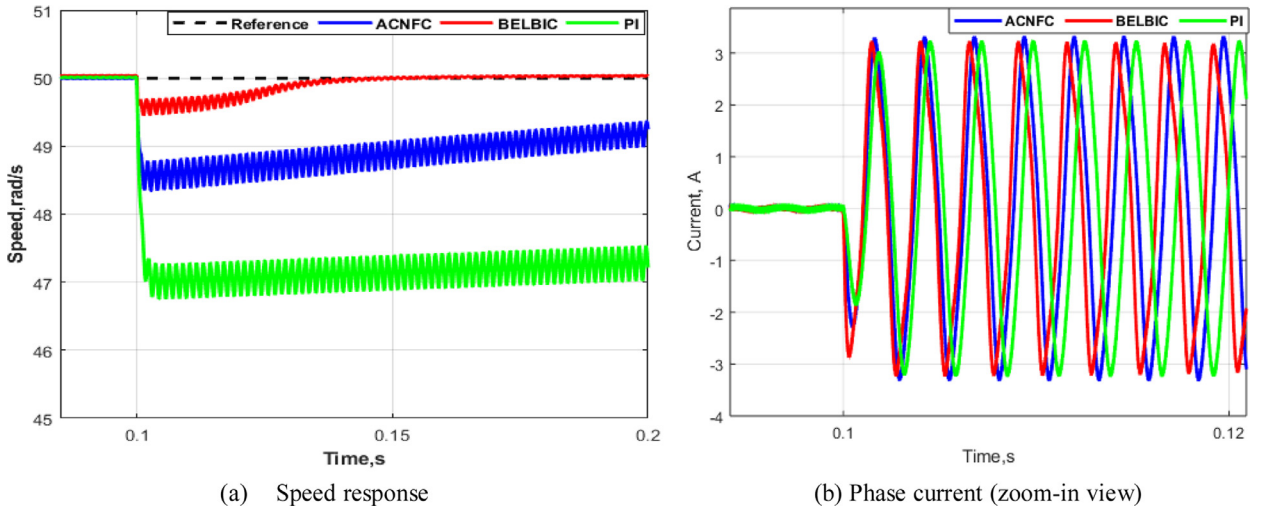


Fig. 7. The speed and current responses of the ACNFC, BELBIC, and PI controllers under impact of the constant load torque disturbance.

the criterion of high-precision tracking that is $\pm 2.5\%$ tracking error with respect to the set point trajectory, in less than 12% simulation time. This performance is comparable with BELBIC which demonstrates fast and accurate response [15]. In this scenario, the optimized-PI controller shows a slower response.

4.2. Scenario II: load-torque disturbance

In this scenario, sudden load torque changes, in two forms of constant and incremental, are applied on the HSM to investigate the ACNFC performance in maintaining stability and disturbance handling. In the first experiment, the HSM operates in the startup mode and a load torque of 0.7 Nm is applied at $t = 0.1$ s (constant load scenario). In the second experiment, the sudden load torque is applied to the HSM in an incremental form as tabulated in Table 2. Figs. 7 and 8 illustrate the impact of the abrupt disturbances on trajectory tracking performance of the ACNFC and the benchmark controllers.

Fig. 7a shows that the ACNFC tracking performance is slightly affected by the constant load torque, about 1.5 rad/sec deviation with respect to the final value of the reference trajectory, at $t = 0.1$ s. However, the adaptation law in ACNFC

Table 2
Characteristics of two types of the load torque disturbances.

Type	Applied Time	Load Condition
Constant	0.1 s	0.7 Nm
Incremental	0.1 s and 0.15 s	0.7 Nm and 1.4 Nm

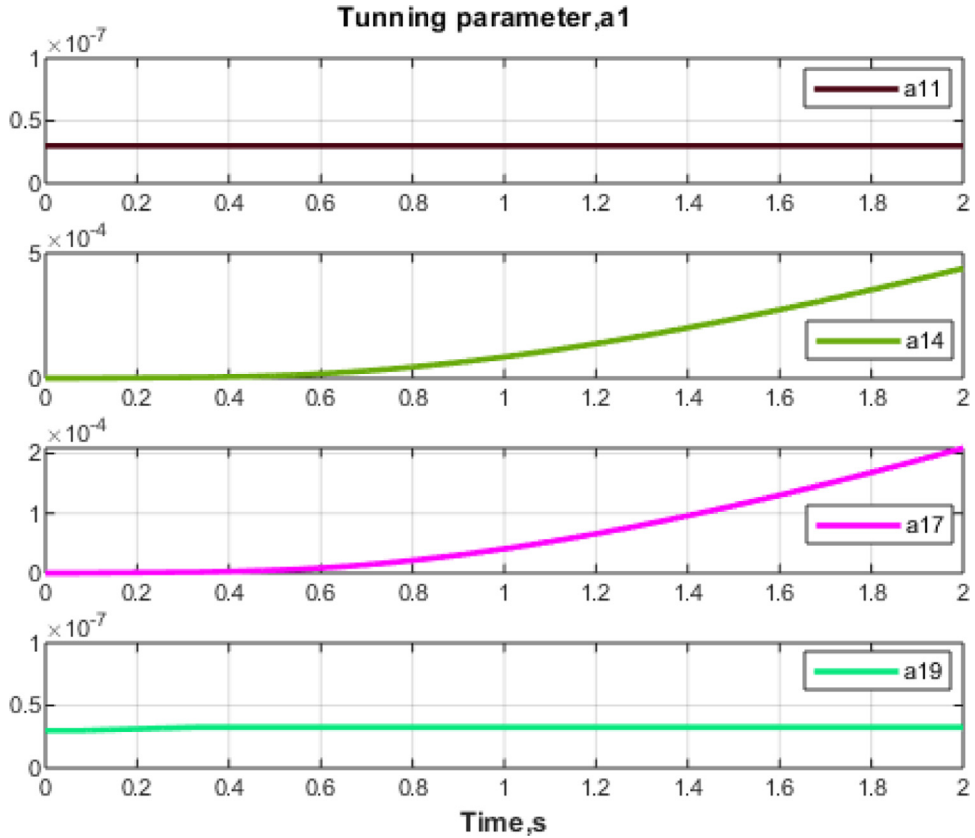


Fig. 8. Selected update of ACNFC tuning parameter, a_{1j} ($j = 1\dots9$), under impact of the constant load torque disturbance.

contributes for correction of the deviation error and recovery of the controller performance to attain less than 1 rad/sec error at $t = 0.2$ s of simulation time. This indicates the fact that the ACNFC can meet the criterion of $\pm 2.5\%$ tracking error even under impact of the constant load torque disturbance. Comparing to the PI performance, the ACNFC speed response in this scenario is more robust and tractable with no extra stator phase current (see Fig. 7b). PI controller shows the maximum deviation around 1.9 rad/s at $t = 0.1$ s with intact tracking error until the end of simulation time. Comparing to the BELBIC, the adaptation law of the ACNFC shows a bit slower response to the sudden load torque and requires more recovery time to mitigate the SSE.

Fig. 8 illustrates the update trend of the ACNFC parameter, a_{1j} indicated in (29). The figure includes two parameters of the most active rules, which experience significant changes, in conjunction with two parameters of non-active rules experiencing fewer changes. As the ACNFC encounters the impact of load torque disturbance, the controller learns a new rule and the critic signal updates the tuning parameters. This can be observed by change of a_{11} to a_{14} and a_{17} and consequently returning to a_{19} .

Fig. 9a and b show the speed response of the ACNFC and benchmark controllers and variations of HSM phase current under the impact of the incremental load change, respectively. Compare to the previous scenario, the impact of incremental load disturbance is more devastating in both speed response and torque ripple as well as the motor phase current with approximately twice stator phase current at $t = 0.15$ s (it requires higher inverter rating in the driver system). In such an aggressive condition, the ACNFC can still maintain the HSM stability and synchronization and hence handle the unknown applied load torque in two sequences of the simulation time. The ACNFC speed response experiences around less than 5% tracking error under impact of the incremental load disturbance at $t = 0.15$ s. In such an unforeseen situation, the critic agent quickly tunes the consequence parts of the neuro-fuzzy structure for adaptation and the control signal tracks the reference trajectory to reach the ACNFC response to the steady-state value of 50 rad/sec. In this scenario, the ACNFC tracking performance is significantly more robust and tractable comparing to that of the PI controller which shows around 12.5% tracking error, with the maximum stator phase current value of around 6.2 A like the ACNFC. However, PI controller has no recovery capacity that may result in losing the HSM steps and hence instability.

Comparing to the BELBIC which shows quick performance in disturbance rejection, the auto-learning of the ACNFC acts slower because of the multi-layer structure of the neuro-fuzzy network.

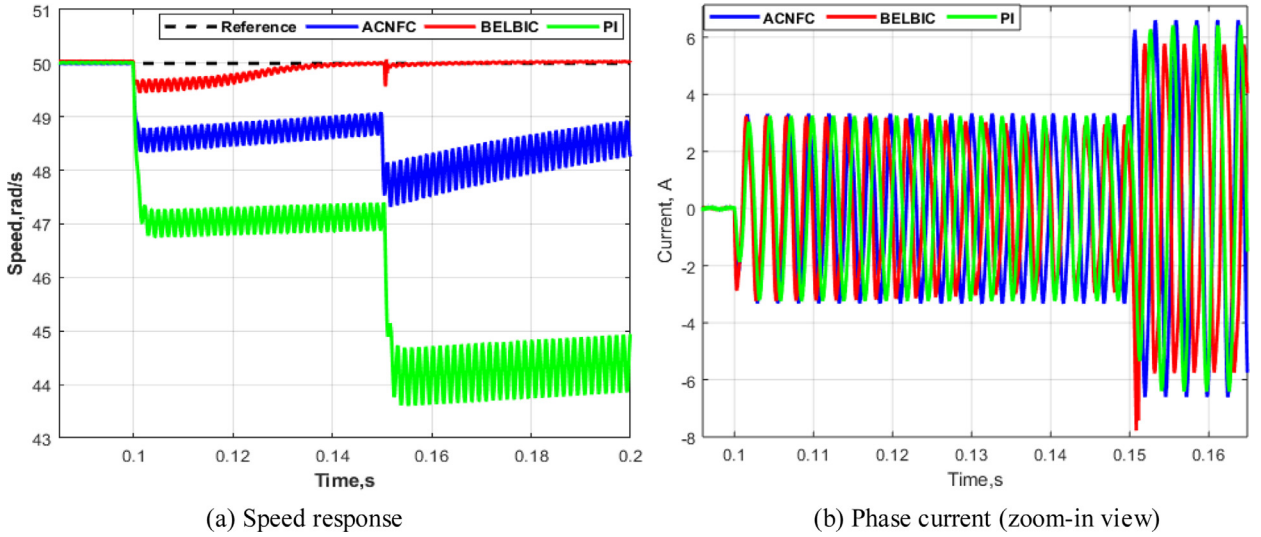


Fig. 9. The speed and current responses of the ACNFC, BELBIC, and PI controllers under impact of the incremental load torque disturbance.

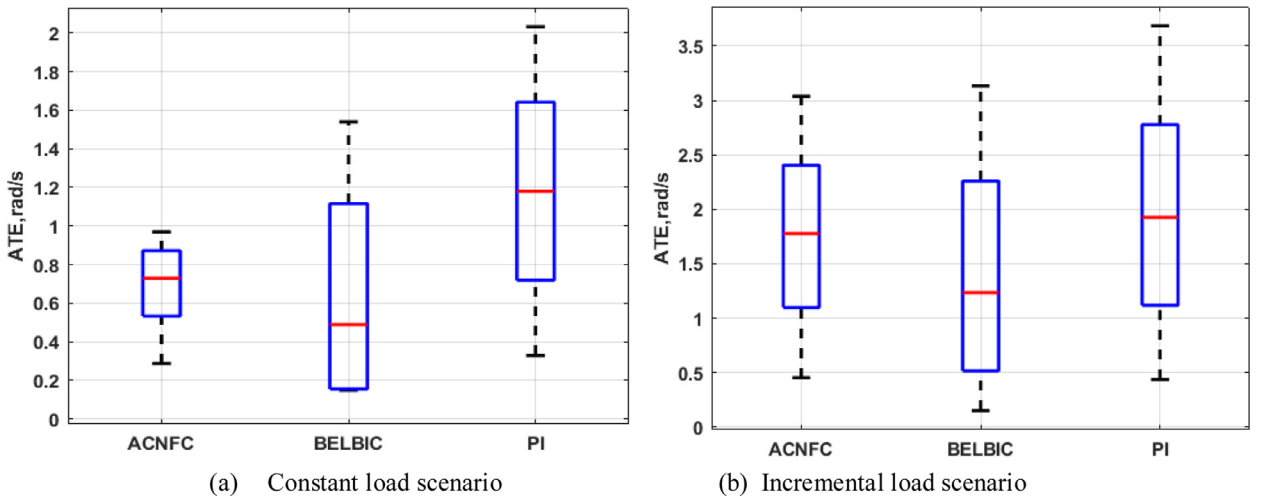


Fig. 10. Robustness assessment of the studied controllers under constant and incremental load scenarios.

To further assess the robustness of the ACNFC and determine its effectiveness in tracking of the speed trajectory, a series of Monte Carlo (MC) simulations with varying load torque is conducted. A set of 20 MC trials with a variable load torque disturbance normally distributed as $\mathcal{N} \sim (1, 1)$ is applied to the HSM operation in both forms of constant and incremental torques. The average tracking error (ATE) is calculated over all experiments.

Fig. 10a and b illustrate statistical analysis of the robustness performance of the ACNFC and benchmark controllers. Box plots in Fig. 10a indicate that the robustness of the ACNFC to a distribution of constant load torque disturbance is roughly twice better than that of PI controller. Even though the median of ATE in the ACNFC performance is about 0.3 rad/sec larger than that of the BELBIC, the variances of ACNFC with respect to the load uncertainty is smaller and more persistent as compared to both BELBIC and PI controllers. This indicates that the error of tracking does not grow exponentially and the probability of losing stability and steps is lower for ACNFC in response to unforeseen load torques. Fig. 10b confirms that all studied controllers' performances degrade with applying a distribution of incremental load torque. In this scenario, the median ATE obtained by the ACNFC still satisfies the criterion of high-precision tracking that is $\pm 2.5\%$ tracking error. The ACNFC variances with respect to load uncertainties are still more robust compared to the BELBIC and PI (even though its median of tracking is about 1 rad/sec larger than that of BELBIC). It should be noted that BELBIC and ACNFC controllers have different architecture structures and use different learning/ adaptation algorithms that leads to different performances.

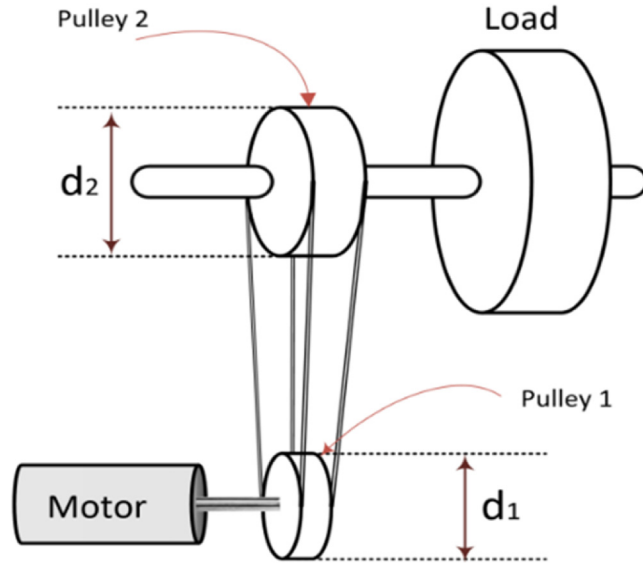


Fig. 11. Attached mechanical setup to the motor shaft.

4.3. Scenario III: uncertainty of the model parameters

In this scenario, robustness assessment of the ACNFC is considered under HSM parameter variations. To this end, the HSM is coupled with a mechanical setup as depicted in Fig. 11. The proposed mechanical components result in the variation of the inertia parameter in the dynamic model of the HSM. This configuration comprises two pulleys, with different diameters, in which the small one is directly coupled to the motor shaft and a belt connects the small pulley to the large one. The load is then joined to the large pulley, and the motor torque is transmitted through the belt and pulleys to drive the load. Eq. (31) represents the equivalent inertia of the HSM in this experiment [15].

$$J_{eq} = \left(\frac{d_1}{d_2} \right)^2 J_2 + J_1 \quad (31)$$

where J_{eq} is the total equivalent inertia on the motor shaft, d_1 and d_2 are the diameters, and J_1 and J_2 are the inertias of the small and large pulleys, respectively.

Table 3 lists the equivalent inertias and loads under two different uncertain conditions to examine the performance of the ACNFC controller against the uncertainty of the model parameters. In Table 3, variations of the nominal HSM inertia to the equivalent inertia are as per the Eq. (31). In a moderate uncertain condition, the inertia is increased to 20% and the HSM is driven under a 0.4-Nm load. In an aggressive uncertain condition, the inertia is doubled and the HSM is driven under a 0.7-Nm load.

Figs. 12 and 13 demonstrate the results of ACNFC and benchmark controllers speed response for uncertain moderate and uncertain aggressive conditions, respectively. In each case, the zoomed-in view of different time intervals is provided to show the controllers undershoot, rise time, recovery process, and SSE of the speed response. Fig. 12a shows the tracking performance of the controllers under an inertia of 1.2 J and load of 0.4 Nm for 0.6 s simulation time. It is inferred from the undershoot at the beginning of speed trajectory that the new coupled system is a non-minimum phase system and therefore the trajectory tracking becomes complicated. Highlighted in Fig. 12b, the ACNFC demonstrates less lag and sensitivity to the non-minimum phase nature of the coupled system by showing less undershoot comparing to both BELBIC and PI controllers. This superior performance is valid for rise time metric as shown in Fig. 12c and d indicates the auto-learning and self-adjustment ability of the ACNFC for uncertainty handing by quick recovery of speed response in less than 0.25 s and reaching to the desired 50 rad/sec speed as shown in Fig. 12e. This quick recovery of the ACNFC and delivering around zero SSE in presence of uncertainty is far more significant comparing to the benchmark controllers' performance.

Table 3

The equivalent inertia and load under uncertain conditions.

Type	Inertia	Load	Simulation time
Moderate uncertain condition	$J \rightarrow 1.2J$	0.4 N.m	0.6 s
Aggressive uncertain condition	$J \rightarrow 2J$	0.7 N.m	0.6 s

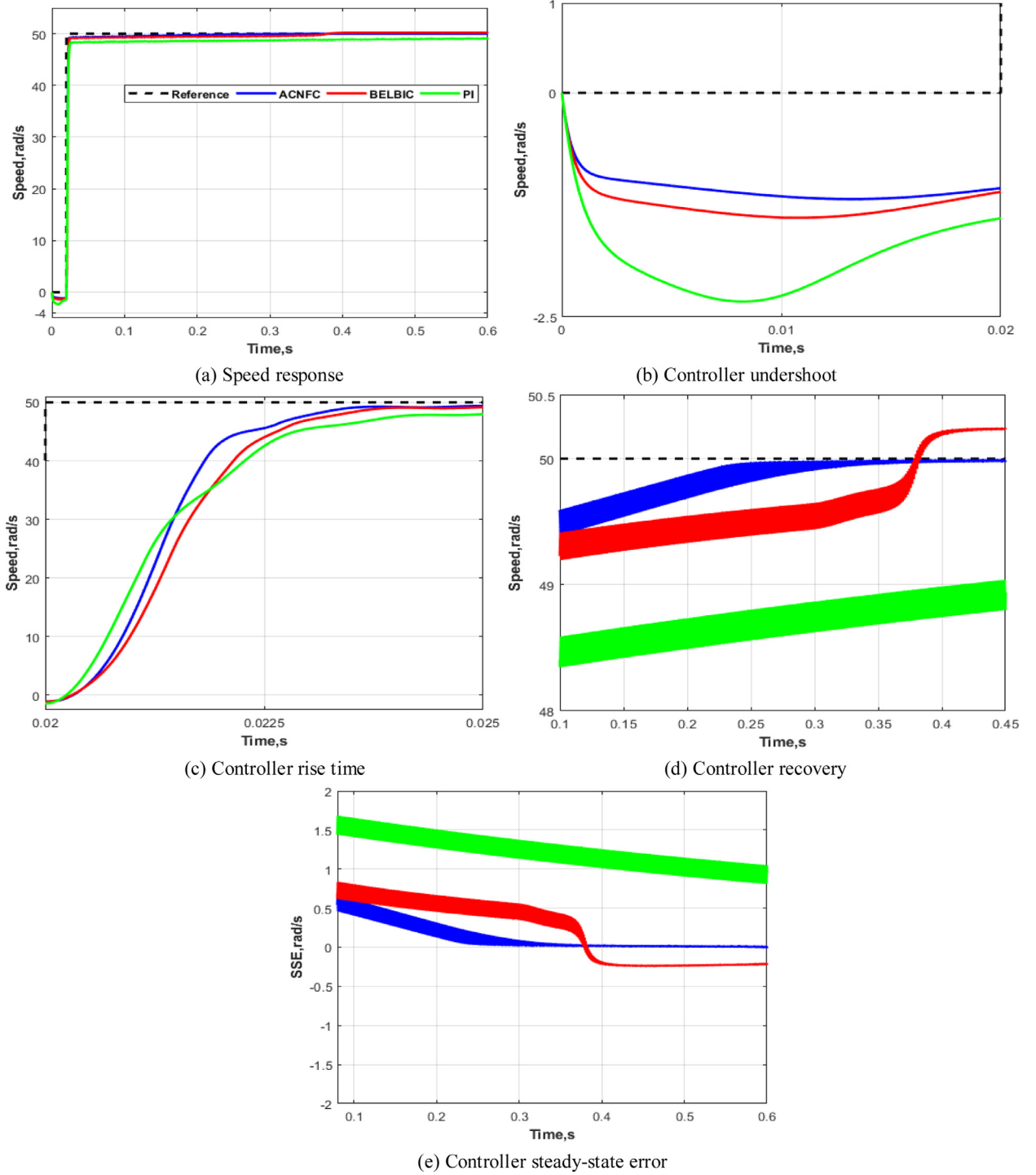


Fig. 12. Tracking performance of the studied controllers under the inertia of 1.2 J and load = 0.4 Nm.

Fig. 13a shows the tracking performance of the studied controllers under an inertia of 2 J and load of 0.7 Nm for 0.6 s simulation time. In dealing with the aggressive uncertain conditions, the uncertainty of the non-minimum phase coupled HSM system applies more destructive impact on the performance of the ACNFC and benchmark controllers compared to the previous scenario. In this scenario, the ACNFC still shows superior performance in terms of the controller undershoot (**Fig. 13b**), recovery capability (**Fig. 13c**), and SSE metric (**Fig. 13d**) as compared to other counterparts. The PI controller is largely at mercy of the parametric uncertainty and cannot compensate the degradation due to its rigid structure and

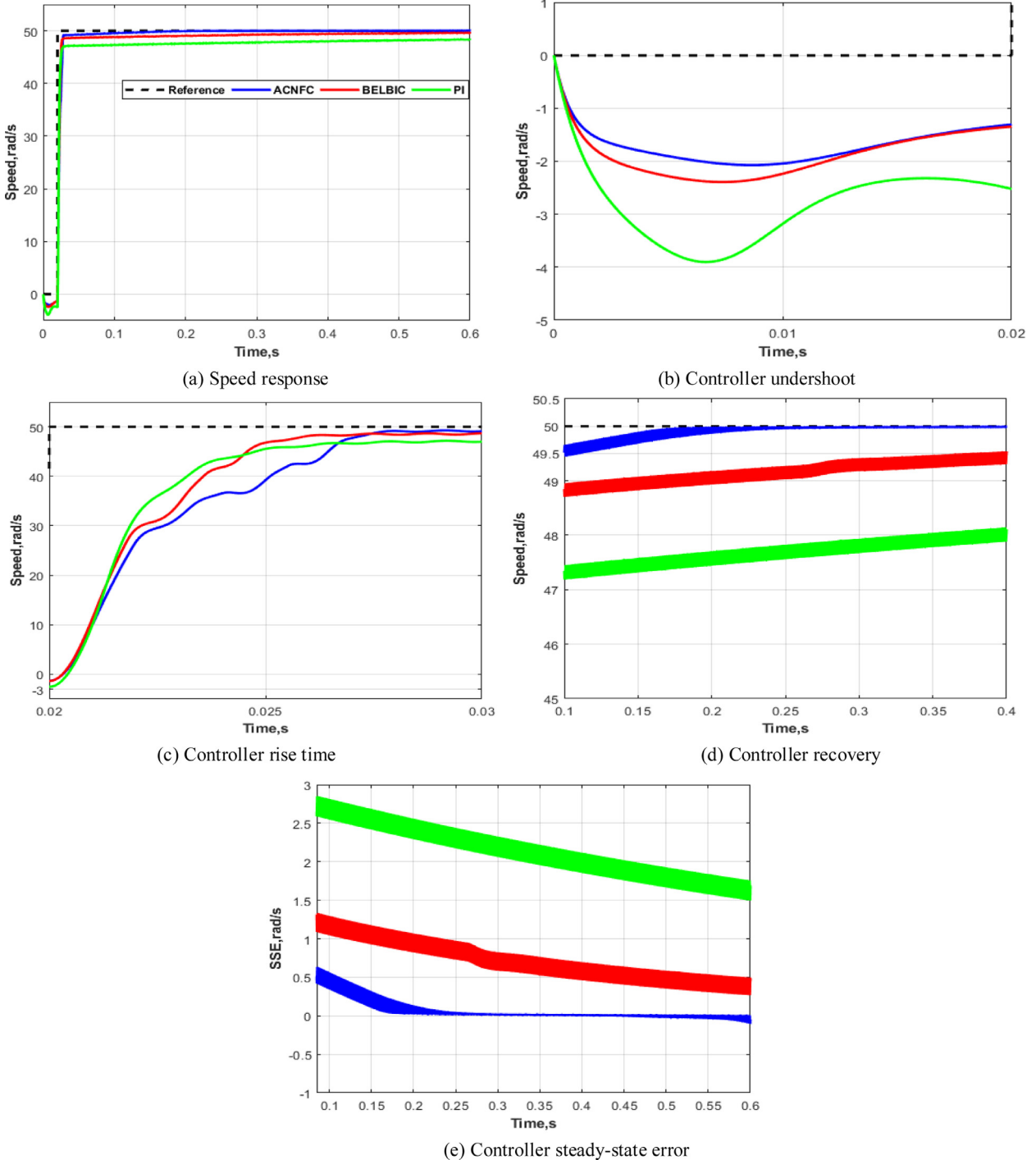


Fig. 13. Tracking performance of the studied controllers under the inertia variation $J \rightarrow 2J$ and load = 0.7 Nm.

lack of adaptability. It is obvious in terms of deviation from the reference and SSE (Fig. 13e). Since the PI controller is an excellent and reliable controller for most of the industrial applications, an optimized-PI controller was selected in this study to benchmark the performance of the proposed ACNFC against uncertainties.

Table 4 quantitatively compares the performance of the ACNFC with the benchmark controllers for two scenarios explained in this section. For this purpose, two performance indices called integral absolute error (IAE), and SSE are calculated in each experiment. As numerically indicated in Table 4, the ACNFC outperforms the benchmark controllers in terms of

Table 4

The performance comparison of studied controllers under moderate and aggressive uncertain operating conditions.

Experiment	Controllers	Integral Absolute Error (IAE)	Steady-State Error (SSE)
Moderate Uncertain Condition	PI	0.5401	0.815
	BELBIC	0.3515	0.212
	ACNFC	0.1920	0.0021
Aggressive Uncertain Condition	PI	0.9237	1.288
	BELBIC	0.5982	0.456
	ACNFC	0.2519	0.0471

transient and steady-state tracking errors in both scenarios. For example, in the moderate uncertain condition, the ACNFC shows approximately 64% and 43% better IAE comparing to the PI and BELBIC, respectively. In terms of SSE, the ACNFC demonstrates around two orders of magnitude better performance comparing to the benchmark counterparts. This significant performance stems from the adaptive structure of the ACNFC supported with auto-learning capability allowing to robustly maintain the HSM synchronization and stability without losing the steps and making the ACNFC a good candidate against unforeseen inertia variations ($J \rightarrow 1.2 \text{ J}$ and $J \rightarrow 2 \text{ J}$).

4.4. Scenario IV: phase interruption

In this scenario, the robustness of the ACNFC against current phase interruption is investigated. Common faults usually occur on the inverter legs of the HSM driver that results in loss of transistor in the driver module and hence loss of one of the motor phases. In this situation, one of the HSM phases is open-circuited causing a loss of field orientation, speed oscillations, torque pulsations, and current and torque distortion. To simulate such an open-circuited condition, the HSM stator current feedback is interrupted at $t = 0.1 \text{ s}$ under the same speed trajectory (50 rad/sec) and full torque load of 0.4 Nm. Fig. 14 shows the speed response of the ACNFC and benchmark controllers under the phase interruption. The effect of open-circuit fault on net torque leads to the increase of torque ripple under fault condition as compared to pre-fault status. This results in increase of speed ripple from about 0.25 rad/sec for all controllers at pre-fault to a maximum value of about 1.7 rad/sec for the ACNFC and BELBIC and a maximum value of about 2.1 rad/s for the PI controller, under the fault condition. It is to be noted that since that inertia of such motor is low ($J = 15.62e-5 \text{ kg.m}^2$) the torque ripple and hence speed ripples are rather high in such fault conditions. Adaptation law updated by the critic-agent in ACNFC (see an example of update of parameters in Fig. 15) leads to acceptable robustness against phase interruption by quick mitigating the speed ripple and maintaining the stability to avoid sever vibration like the BELBIC.

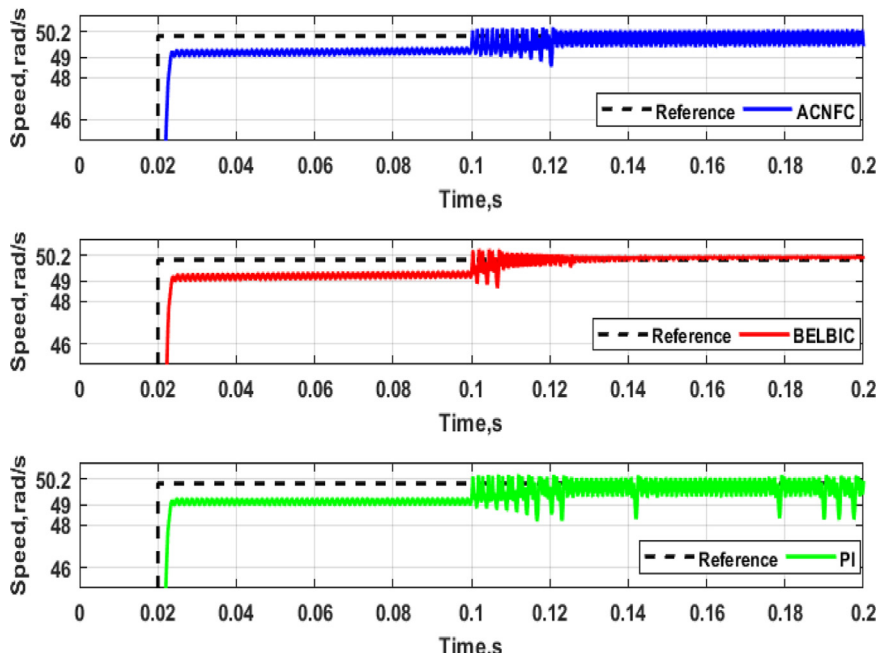


Fig. 14. Performance of the ACNFC, BELBIC, and PI controllers under sudden phase current fault/interrupt.

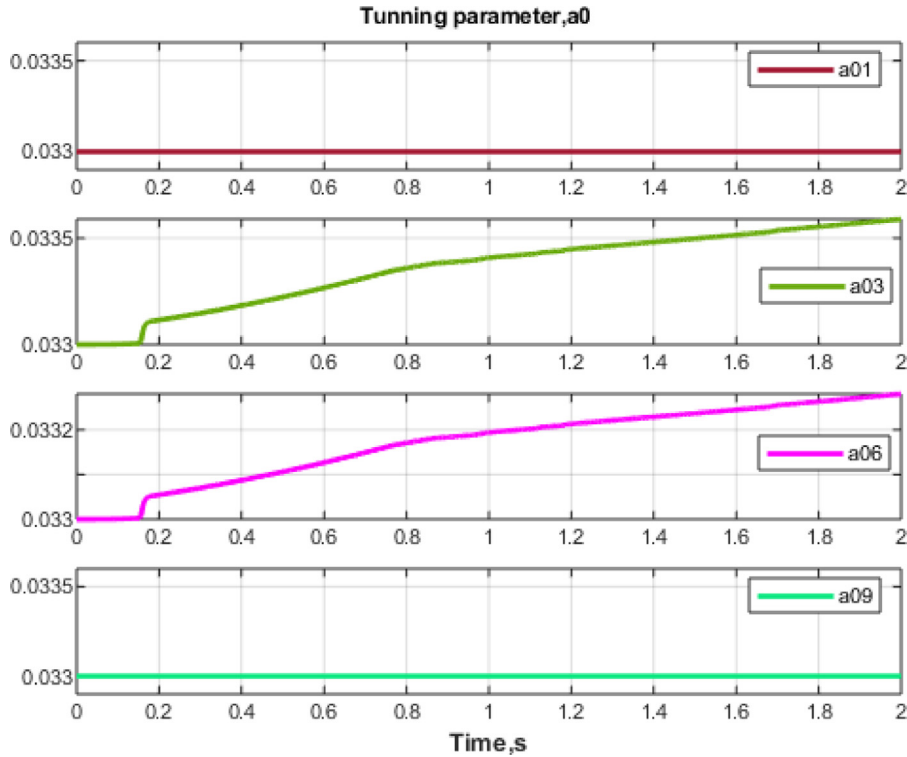


Fig. 15. Selected update of ACNFC tuning parameter, a_{0j} ($j = 1, \dots, 9$), under impact of sudden phase current fault/interrupt.

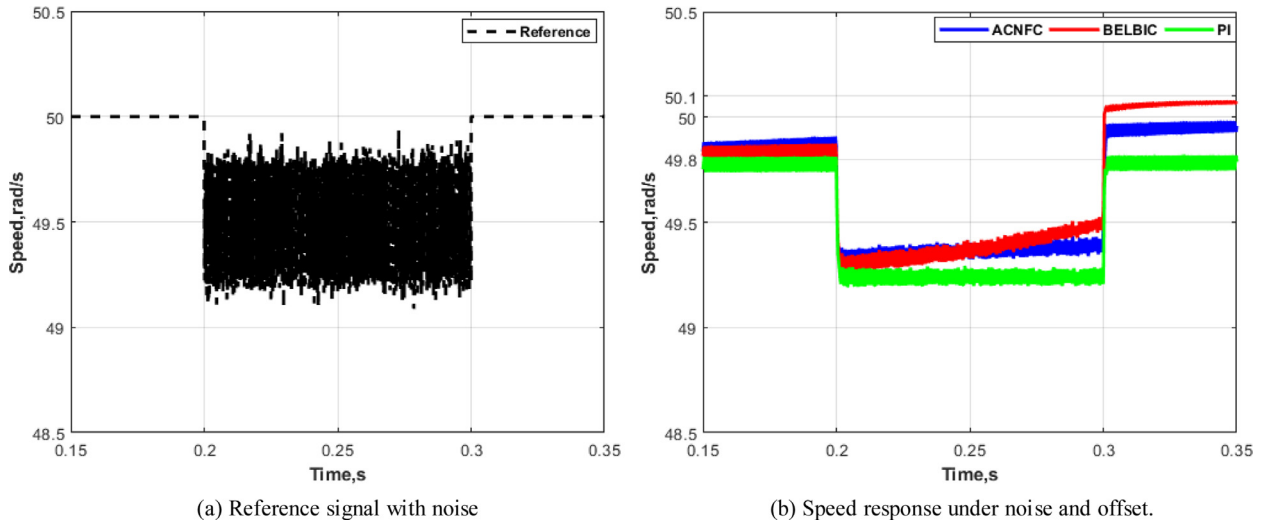


Fig. 16. Noise and offset signal applied to the HSM drive system under rated speed 50 rad/s and rated load condition 0.1 Nm.

4.5. Scenario V: noise impact

In this scenario, capacity of the ACNFC to handle unforeseen noise and offset on the HSM system is investigated. The noise and offset can be due to a malfunction of measurement sensors such as encoder or tachometer or impact of environmental disturbances produced by power electronic elements/devices such power supplies, on the feedback loop. To simulate the impact of noise and offset on the HSM speed response, a white noise signal $\mathcal{N} \sim (0, 0.01)$ with 1% offset is added to the reference speed signal. In this experiment, a torque load of 0.1 Nm is coupled with the motor shaft.

Fig. 16a illustrates the noise and offset signal applied to the reference speed trajectory and Fig. 16b shows the speed response of the ACNFC and benchmark controllers in this situation. It is obvious from Fig. 16b that the ACNFC is robust

enough against noise and offset; relying on its adaptation law, it can quickly return to set point of 50 rad/sec and eliminates the SSE. This performance is superior comparing to the studied benchmark controllers.

5. Conclusion

The ACNFC was developed for high-precision speed trajectory tracking of the HSM. The effectiveness and robustness of the controller were examined under model parameter variation, load disturbance, noise impact, and sudden fault occurrence. The controller performance was evaluated against optimized-PI and BELBIC controllers as benchmark controllers. The simulation results showed that the ACNFC is able to meet the precision criterion of tracking and handling uncertainties. The ACNFC performance success stemmed from the critic-based learning algorithm assessing the system performance and tuning the parameters of the controller. This makes the ACNFC adaptive and reconfigurable so that it can eliminate the resonance and vibration phenomenon at different operating conditions, diminish the torque ripple quickly, and maintain the stability, synchronization and steps of the HSM even against sudden load torque disturbances, noise impacts, and inertia variations.

Future work will involve the ACNFC implementation on a laboratorial HSM platform (currently under development) with the purpose to validate the effectiveness and robustness of the ACNFC in real-world experiments and compare its performance with other controllers namely state-feedback decoupling and complex-vector controllers. Moreover, fidelity and effectiveness of the ACNFC controller for high precision simultaneous position and speed tracking of robot manipulators equipped with the visual attention technology [25] will be investigated.

Declaration of competing interest

None.

CRediT authorship contribution statement

P. Ghanooni: Conceptualization, Methodology, Formal analysis, Software, Validation. **A.M. Yazdani:** Conceptualization, Formal analysis, Validation, Supervision, Writing - original draft, Writing - review & editing. **A. Mahmoudi:** Formal analysis, Validation, Writing - review & editing. **S. MahmoodZadeh:** Software, Visualization. **M. Ahmadi Movahed:** Software, Validation. **M. Fathi:** Resources.

References

- [1] Butcher M, Masi A, Picatoste R, Giustiniani A. Hybrid stepper motor electrical model extensions for use in intelligent drives. *IEEE Trans Indust Electron* 2014;61(2):917–29.
- [2] Daouda M, Lin CL, Lee CS, Yang CC, Chen CA. Model predictive control of sensorless hybrid stepper motors in auxiliary adjuster for stereotactic frame fixation. *Mechatronics* 2017;47:160–7.
- [3] Arias A, Caum J, Ibarra E, Grinó R. Reducing the cogging torque effects in hybrid stepper machines by means of resonant controllers. *IEEE Trans Indust Electron* 2019;66(4):2603–12.
- [4] Tran HN, Le KM, Jeon JW. Adaptive current controller based on neural network and double phase compensator for a stepper motor. *IEEE Trans Power Electron* 2018.
- [5] Le KM, Van Hoang H, Jeon JW. An advanced closed-loop control to improve the performance of hybrid stepper motors. *IEEE Trans Power Electron* 2017;32(9):7244–55.
- [6] Zribi M, Chiasson J. Position control of a PM stepper motor by exact linearization. *IEEE Trans Automat Contr* 1991;36(5):620–43.
- [7] Betin F, Deloizy M, Goelde C. Closed loop control of a stepping motor drive comparison between PID control, self-tuning regulation and fuzzy logic control. *EPE J* 1999;8(1–2):33–9.
- [8] Gaan DR, Kumar M, Sudhakar S. Real-time precise position tracking with stepper motor using frequency modulation based microstepping. *IEEE Trans Ind Appl* 2018;54(1):693–701.
- [9] Lee Y, Shin D, Kim WH, Chung CC. Proximate in-phase current estimator to reduce torque ripple in permanent-magnet stepping motor. *IEEE Trans Indust Electron* 2016;63(3):1707–16.
- [10] Nollet F, Floquet T, Perruquetti W. Observer-based second order sliding mode control laws for stepper motors. *Control Eng Pract* 2008;16(4):429–43.
- [11] Ahmadi A, Sedehi MT, Yazdani AM, Haniff MF, Buyamin S, Rahim HA. Designing an optimal fuzzy-PID controller for speed tracking of stepper motor. In: Industrial Electronics and Applications (ISIEA), 2012 IEEE Symposium on. IEEE; 2012. p. 193–8.
- [12] Yazdani AM, Ahmadi A, Buyamin S, Rahmat MFA, Davoudifar F, Rahim HA. Imperialist competitive algorithm-based fuzzy PID control methodology for speed tracking enhancement of stepper motor. *Int J Smart Sens Intell Syst* 2012;5(3).
- [13] Rubaai A, Kotaru R. Adaptation learning control scheme for a high-performance permanent-magnet stepper motor using online random training of neural networks. *IEEE Trans Ind Appl* 2001;37(2):495–502.
- [14] Yazdani AM, Buyamin S, Mahmoodzadeh S, Ibrahim Z, Rahmat M. Brain emotional learning based intelligent controller for stepper motor trajectory tracking. *Int J Phys Sci* 2012;7(15):2364–86.
- [15] Yazdani AM, Mahmoudi A, Movahed MA, Ghanooni P, Mahmoodzadeh S, Buyamin S. Intelligent speed control of hybrid stepper motor considering model uncertainty using brain emotional learning. *Can J Electric Comp Eng* 2018;41(2):95–104.
- [16] Betin F, Pinchon D, Capolino G-A. Fuzzy logic applied to speed control of a stepping motor drive. *IEEE Trans Indust Electron* 2000;47(3):610–22.
- [17] Rubaai A, Castro-Sitiriche MJ, Garuba M, Burge L. Implementation of artificial neural network-based tracking controller for high-performance stepper motor drives. *IEEE Trans Indust Electron* 2007;54(1):218–27.
- [18] Berenji HR, Khedkar P. Learning and tuning fuzzy logic controllers through reinforcements. *IEEE Trans Neural Netw* 1992;3(5):724–40.
- [19] Fakhrazari A, Boroushaki M. Adaptive critic-based neurofuzzy controller for the steam generator water level. *IEEE Trans Nucl Sci* 2008;55(3):1678–85.
- [20] Farhangi R, Boroushaki M, Hosseini SH. Load-frequency control of interconnected power system using emotional learning-based intelligent controller. *Int J Electr Power Energy Syst* 2012;36(1):76–83.
- [21] Hatami E, Vosoughi N, Salarieh H. Design of a fault tolerated intelligent control system for load following operation in a nuclear power plant. *Int J Electr Power Energy Syst* 2016;78:864–72.
- [22] Zaky MS, Ismaeil EM, Khater MM. Gain scheduling adaptive proportional-integral controller for a field-oriented control of hybrid stepper motor drives. *Electric Power Compon Syst* 2012;40(7):777–91.

- [23] Rahmat MFA, Yazdani AM, Movahed MA, Mahmoudzadeh S. Temperature control of a continuous stirred tank reactor by means of two different intelligent strategies. *Int J Smart Sens Intell Syst* 2011;4(2).
- [24] Movahed MA, Yazdani AM. Application of imperialist competitive algorithm in online PI controller. In: Intelligent Systems, Modelling and Simulation (ISMS), 2011 Second International Conference on. IEEE; 2011. p. 83–7.
- [25] Pan Z, Liu S, Sangaiah A, Muhammad K. Visual attention feature (VAF): a novel strategy for visual tracking based on cloud platform in intelligent surveillance systems. *J Parallel Distrib Comput* 2018;120:182–94.

P. Ghanooni received the bachelor's degree in electronic engineering from Islamic Azad University, Naeen Branch, Esfahan, Iran, in 2007, and the master's degree in control engineering from Islamic Azad University, Mashhad branch, Mashhad, Iran, in 2011. His current research interests include robotic and mechatronic systems, industrial control and automation, and intelligent control applications.

A.M. Yazdani received the master's degree in control engineering from Universiti Teknologi Malaysia, Johor Bahru, Malaysia, in 2012, and the Ph.D. degree in control engineering from Flinders University, Australia, in 2017. He is currently working as a Lecturer in Electrical Engineering at Murdoch University, Australia. His current research interests include robotic and mechatronic systems, optimal and nonlinear control, electrical drives, and intelligent control applications.

A. Mahmoudi received the bachelor's degree in electrical engineering from Shiraz University, Iran, in 2005, the master's degree in electrical power engineering from Amirkabir University of Technology, Iran, in 2008, and the Ph.D. degree from University of Malaya, Kuala Lumpur, Malaysia, in 2013. He is currently a Lecturer of Electrical Engineering with Flinders University, Australia. His current research interests include the modelling and design of electrical machinery.

S. Mahmoudzadeh received her Ph.D. degree in computer science from Flinders University, Australia, in 2017. She is currently working as a Lecturer in Data Science at Deakin University, Australia. Her current research interests include computational intelligence, autonomy and decision-making, and situational awareness.

M. Ahmadi Movahed received the master's degree in mechatronic and automatic control from Universiti Teknologi Malaysia, Malaysia, in 2011. He is currently pursuing toward Ph.D. degree in control engineering with Islamic Azad University, Science and Research Branch, Tehran, Iran. His current research interests include intelligent, adaptive, and nonlinear control theories and applications.

M. Fathi received his bachelor's degree from Islamic Azad University, Khomeini Shahr branch, Iran, and his master's degree from Universiti Teknologi Malaysia, both in electrical-power engineering, in 2005 and 2011 respectively. He is currently working as an Engineer Designer, Counselor and Supervisor at Moshanir Consultant Company, Iran. His area of research includes power system modelling and optimization, smart power system control, and electrical drives.